

## Design optimization of a flexural hinge-based bender for X-ray optics

L. Zhang,\* R. Hustache, O. Hignette, E. Ziegler and A. Freund

European Synchrotron Radiation Facility, BP 220, 38043 Grenoble CEDEX, France. E-mail: zhang@esrf.fr

(Received 4 August 1997; accepted 3 November 1997)

This paper presents a parameter study and design optimization of a flexural hinge-based bender by use of finite-element modelling and analytical formulation. The relationship between the mirror shape and the driving forces, the so-called bender driving equation, is established. Various parameters are investigated: the material properties, the geometrical parameters, the stress and deformation of the mirror and flexural hinge, the residual slope error of the mirror, and the resolution required for the actuators. Analysis results have been compared with test results for a prototype bender and a silicon mirror (170 × 40 × 10 mm). Both analysis and test results confirm the microradian accuracy of the bent mirror. Finally, a bender design for short-bending-radius applications is also presented.

**Keywords:** X-ray optics; elliptical mirrors; dynamical benders; flexural hinges.

### 1. Introduction

Dynamical bending devices for focusing X-ray optics in synchrotron radiation applications are attractive development subjects. Such devices respond to the energy tunability requirements, and can possibly be used to correct thermal deformation of the optical surface. Mechanical benders have mostly been used for this purpose. A cylindrical shape can be achieved by using a mechanical or a pneumatical bender (developed by Carl Zeiss, D-7082 Oberkochen, Germany) with identical moments applied at the end of a rectangular mirror, or by applying identical forces at the end of a crystal of variable width (Müllender *et al.*, 1995, 1997) or variable thickness. Elliptical bending X-ray mirrors can be produced by applying equal or unequal moments to a mirror of

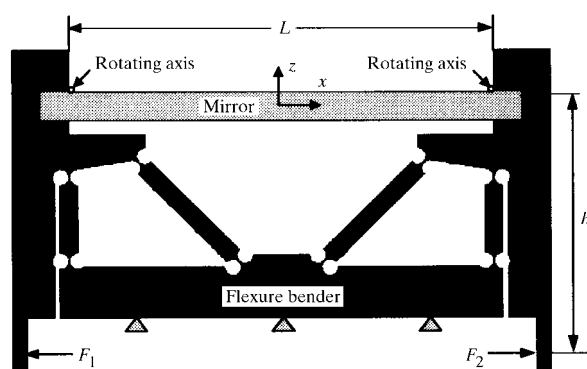


Figure 1

Finite-element model of the flexural hinge-based bender for the multilayer mirror. The piezo actuators are illustrated by two arrows. Triangles represent fixations.

variable width (Padmore *et al.*, 1996) or variable thickness (Howells & Lunt, 1993). A piezoelectric bimorph mirror (Susini *et al.*, 1994; Zhang *et al.*, 1994) has also been developed for dynamical bending of synchrotron radiation mirrors (Signorato *et al.*, 1998).

As a small focal spot is often required, it is more and more difficult to apply the moment or force with sufficient accuracy. Padmore *et al.* (1996) have discussed the fact that unintended additional forces may be applied to the mirror by some benders and compromise the optical performance. Flexural hinges have been introduced in the bender design to minimize unintended additional forces. A bender using flexural hinges has been developed for crystal bending by Henins (1987). One rotational axis and one stationary axis were used to produce cylindrical bending with changeable radius of curvature. Two-rotational-axes bending devices have been designed at the ESRF by Hustache (Freund, 1992; Krisch, 1993) for thin-crystal bending application, and modified to bend multilayer optics and thick mirror substrates (Ziegler, 1995; Ziegler *et al.*, 1996). Howells & Lunt (1993) have also used the flexural hinge in the monolithic design of mirror benders. Design strategies for a monolithic adjustable-radius metal mirror have been discussed by Howells (1995).

This paper deals with the analysis of the flexural hinge bender used at the ESRF for multilayer optics and a thick substrate of mirrors by analytical formulation and finite-element analysis. A two-dimensional model of the prototype bender for multilayer optics with actuators is shown in Fig. 1. The multilayer optics are 170 mm long, 50 mm wide and 10 mm thick (Ziegler, 1995). The width of the bender is also 50 mm. The clamped length of the mirror is 10 mm. The useful length of the optics is then  $L = 150$  mm. The pushing forces  $F_1$  and  $F_2$  are applied by two piezo actuators. This prototype bender has two rotating axes on the top surface of a 10 mm-thick mirror, as indicated in Fig. 1. The length of the bending lever,  $h$ , is 92 mm. The bender with the flexural hinges is cut from a single block of high-strength stainless steel by wire-electric discharge machining. All hinges have the same critical dimensions: thickness  $t_f = 0.14$  mm, cutting radius  $R_f = 3$  mm. Based on this bender, design optimization is made to increase the bending capacity and to reduce the sensitivity of the slope to the accuracy or resolution of the actuators. Test results in the ESRF optics metrology laboratory and on an X-ray beamline will be compared with the results from the analysis. Finally, a new bender design for short-bending-radius applications is presented.

### 2. Modelling of the mirror bender assembly

#### 2.1. Mirror in pure bending condition

Ideally, the bender should apply to the mirror pure-bending moments,  $M_1 = hF_1$  and  $M_2 = hF_2$ . The bending of the mirror can be analysed by using standard mechanical beam theory. The validity conditions for such an analysis have already been discussed by Roark (Young, 1989). The shape of the bent beam under the action of two different moments  $M_1$  and  $M_2$  is defined by the following differential equation (Ugural & Fenster, 1995)

$$d^2z/dx^2 = (h/EI)[(F_1 + F_2)/2 + (F_2 - F_1)x/L], \quad (1)$$

where  $E$  is Young's modulus of the material and  $I = t^3W/12$  is the moment of inertia of a rectangular beam cross section, where  $t$  is the thickness and  $W$  is the width.

**Table 1**Bending-loss factors  $\delta$  and  $\delta_x$  of the mirror bender assembly for both the prototype bender shown in Fig. 2 ( $h_a = 10 - t$ ) and for the modified bender ( $h_a = 0$ ).

Flexure bender		Mirror		$h_a = 10 - t$		$h_a = 0$		$C_0$ (mm <sup>-1</sup> )	$C_x$ (mm <sup>-1</sup> )	$C_N$ (mm <sup>-1</sup> )
$E_f$ (GPa)	$y_f$ (mm)	$E$ (GPa)	$y$ (mm)	$\delta$	$\delta_x$	$\delta$	$\delta_x$			
200	0.14	70	6	0.7687	0.0102	0.0289	0.0101	609	212	58.3
200	0.14	70	8	0.5301	0.0045	0.0126	0.0045	626	225	63.5
200	0.14	70	10	0.3099	0.0027	0.0065	0.0023	636	226	55.8
200	0.14	70	20	0.0009	0.0020	0.0009	0.0020	693	1582	–
200	0.14	110	10	0.2442	0.0016	0.0042	0.0016	647	252	44.2
200	0.14	110	20	0.0006	0.0024	0.0006	0.0024	708	2992	–
200	0.1	70	10	0.2924	0.0009	0.0028	0.0009	636	197	53.3
200	0.21	70	10	0.3323	0.0070	0.0179	0.0067	631	236	57.9
200	0.28	70	10	0.3513	0.0139	0.0360	0.0143	620	246	58.0
66	0.14	70	10	0.1708	0.0005	0.0022	0.0005	660	151	31.0

## 2.2. Bender driving equation

The prototype bender for multilayers and for a thick mirror was tested in the ESRF optics metrology laboratory (Ziegler *et al.*, 1996). The driving forces were applied by two actuators of capacity 100 N. The measured shape of a 10 mm-thick silicon mirror under equal forces is a cylinder with a radius of curvature of 71.1 m. Although the effective force was not measured, such a radius was probably achieved with the actuators close to their maximum capacity. This prototype bender was analysed by finite-element modelling (FEM) with the model shown in Fig. 1. Two equal forces of  $F_1 = F_2 = 1.854$  N per mm were applied to the two-dimensional model; the equivalent force delivered by the actuators is 92.7 N, considering the width of 50 mm of the system. The curvature calculated by the FEM (Fig. 2) has a constant value in the central region of the mirror ( $|x| < 65$  mm) corresponding to a bending radius of  $R = 71.1$  m. The excellent agreement between the results of the FEM and of the test in the ESRF optics metrology laboratory validates the FEM. The results of the FEM clearly show edge effects at the two ends of the mirror within a length equivalent to the mirror thickness, 10 mm in this case. In practice, the mirror length,  $L$ , should be at least 20 mm longer than the X-ray footprint length.

The radius of curvature,  $R = EI/hF = 53.74$  m from (1), for the above case is 24.4% smaller than the experimental and the FEM results. This means that there is some bending-capacity loss in this mirror bender assembly.

From a more detailed mechanical analysis, we deduce that the effective bending moments  $M_{ei}$  ( $i = 1, 2$ ) should be

$$M_{ei} = M_i - M_{fi} - h_a N, \quad i = 1, 2 \quad (2)$$

where  $M_{f1}$  and  $M_{f2}$  are the total reaction bending moments of the four left and the four right flexural hinges,  $h_a$  is the distance

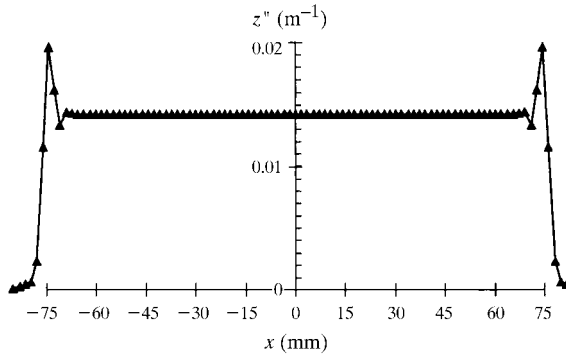


**Figure 2** Curvature distribution from the FEM for a 10 mm-thick silicon mirror, under equal forces  $F_1 = F_2 = 1.854$  N per mm width.

between the neutral plane of the mirror and the rotating axes, and  $N$  is the reactive force applied to the bender by the mirror. The reactive bending moment,  $M_f$ , of a flexural hinge can be calculated from the rotation angle,  $\varphi$ , of the flexural hinge by (Paros & Weisbord, 1965)

$$M_f = k\varphi, \quad k = 2E_f t_f^{5/2} W / 9\pi R_f^{1/2}. \quad (3)$$

Let us introduce the notation  $\varphi_1$  and  $\varphi_2$ , which are the sum of the rotation angles of all the flexural hinges on the left-half part and on the right-half part of the bender, respectively, and the corresponding bending moments  $M_{f1}$  and  $M_{f2}$ . As the rotation angles  $\varphi_1$  and  $\varphi_2$  of the flexural hinges are associated with the deformation of the bender and the mirror, these rotation angles of the flexural hinges can be assumed to be proportional to the curvatures of the mirror at the left end and right end, respectively,

$$\varphi \propto 1/R_i = M_i/EI, \quad i = 1, 2$$

and then

$$M_{f1} = (C_0 + C_x)kM_1/EI, \quad M_{f2} = (C_0 - C_x)kM_2/EI, \quad (4)$$

where  $C_0$  and  $C_x$  are constants depending only on the bender design. When the neutral plane of the mirror is below the two rotating axes, the mirror is under tensile stress. The tensile force  $N$  is proportional to the average force  $(F_1 + F_2)/2$  and approximately proportional to the thickness of the mirror,  $N = C_N t (F_1 + F_2)$ . Substituting  $M_1$  and  $M_2$  by  $M_{e1}$  and  $M_{e2}$  into (1), we obtain the following bender driving equation,

$$\frac{d^2 z}{dx^2} = \left( \frac{h}{EI} \right) \left[ \frac{(F_1 + F_2)}{2} (1 - \delta) + (F_2 - F_1) \frac{x}{L} (1 - \delta_x) \right], \quad (5)$$

with

$$\delta = C_0(k/EI) + C_N(h_a t/h), \quad \delta_x = C_x(k/EI). \quad (6)$$

These two constants represent bending-loss factors of the mirror bender assembly. The finite-element model of the prototype bender has been slightly modified to ensure that the neutral plane of the mirror coincides with the two rotating axes of the bender. The modification was made just on the height of the base to support the mirror. This height was  $15 - t/2$  mm instead of the fixed value of 5 mm. Various parameters of the mirror (thickness  $t$ , material property  $E$ ) and of the flexure bender (hinge thickness  $t_f$ , material property  $E_f$ ) have been studied for both the bender shown in Fig. 1 and for the modified version. The results of bending-loss factors  $\delta$  and  $\delta_x$  are given in Table 1, and the constants  $C_0$ ,  $C_x$  and  $C_N$  are also calculated by (6). Values of  $E$  of 70 and 110 GPa correspond to silica and silicon, respectively. Values of  $E_f$  of 200 and 66 GPa correspond to stainless steel and aluminium, respectively.

The bending-loss factor,  $\delta$ , of the prototype bender is mainly due to the non-coincidence between the neutral plane of the mirror and the rotating axes of the bender ( $h_a \neq 0$ ). This loss factor reaches 0.768 for a 6 mm-thick silica mirror. For the mirror (silicon,  $t = 10$  mm) and flexural hinge (steel,  $t_f = 0.14$  mm) used in the prototype,  $\delta = 0.2443$ , which can be reduced to 0.0042 if the mirror is placed on the rotating axis of the bender.

### 2.3. Ideal elliptical-bending approximation

If a mirror is placed at a distance  $p$  from the X-ray sources with an incidence angle  $\theta$ , and an image is expected at a distance  $q$  downstream of the mirror, the ideal shape of the mirror should be an ellipse, and can be represented by a series of  $x, z$  coordinates in the mirror reference as (Susini, 1992; Padmore *et al.*, 1996)

$$z = \alpha x^2(1 + \beta x + \gamma x^2 + \dots), \quad (7)$$

of which the radius of curvature,  $R(x)$ , is

$$1/R(x) \simeq d^2 z/dx^2 = 2\alpha(1 + 3\beta x + 6\gamma x^2 + \dots), \quad (8)$$

where

$$\begin{aligned} \alpha &= \sin \theta(1 + p/q)/4p, \\ \beta &= \cos \theta(p/q - 1)/2p, \\ \gamma &= 1/4pq + 5\beta^2/4. \end{aligned} \quad (9)$$

For a mirror with constant cross section, a cubic approximation can be made to the elliptical shape by the flexure bender presented here. However, by comparing (5) with the first two terms in (8), the value of the forces  $F_1$  and  $F_2$  can be determined by

$$F_1 = (EI/h)\alpha[2/(1 - \delta) - 3\beta L/(1 - \delta_x)], \quad (10)$$

$$F_2 = (EI/h)\alpha[2/(1 - \delta) + 3\beta L/(1 - \delta_x)]. \quad (11)$$

The cubic approximation is sometimes not sufficient. The variable cross section of the mirror is then necessary to produce an exact ellipse shape. In order to do that, the thickness  $t$  and the width  $W$  of the mirror should be

$$t^3 W = (1 + 3\beta x)t_0^3 W_0/(1 + 3\beta x + 6\gamma x^2 + \dots), \quad (12)$$

where  $t_0$  and  $W_0$  are the initial thickness and initial width of the mirror used to calculate the bending forces by (10) and (11). In practice, only one parameter of the mirror is variable,  $t$  or  $W$ . Considering the tolerance limit when manufacturing and polishing the mirror, a variable width is preferable for a variable cross section of the mirror as discussed by Padmore *et al.* (1996). However, a mirror with a variable cross section allows a perfect ellipse to be approached for single optical configuration, therefore precluding the energy tunability.

### 2.4. Sensitivity to the actuator accuracy

Note that  $\delta > \delta_x$ , and it can be demonstrated that the maximum slope sensitivity,  $\varepsilon_{\theta/F}$ , to the forces is at the end of the mirror,  $x = L/2$  or  $x = -L/2$ , and

$$\varepsilon_{\theta/F} = \left| \frac{\partial \theta}{\partial F_1} \right|_{\max} = \left| \frac{\partial \theta}{\partial F_2} \right|_{\max} = \frac{hL}{8EI}(3 - 2\delta - \delta_x). \quad (13)$$

For the tested prototype bender with a silicon mirror of  $W = 40$ † and  $t = 10$  mm, the sensitivity is  $\varepsilon_{\theta/F} = 11.8 \mu\text{rad N}^{-1}$  from (13).

† This mirror is narrower than the bender.

The displacement of the bender at the forces application points is  $k_{\text{lever}} = 1.37 \mu\text{m N}^{-1}$  from the results of the FEM. The accuracy in force and in displacement of the actuators should be better than  $1/\varepsilon_{\theta/F} = 0.085 \text{ N } \mu\text{rad}^{-1}$  and  $1/\varepsilon_{\theta/D} = k_{\text{lever}}/\varepsilon_{\theta/F} = 0.117 \mu\text{m } \mu\text{rad}^{-1}$ , respectively.

### 3. Comparison with test results

Now let us study a test case in the ESRF BM5 beamline (Hignette *et al.*, 1997). A silicon mirror ( $t = 10$  mm,  $W = 40$  mm,  $L = 150$  mm) with the flexure bender is placed at  $p = 40$  m from the X-ray source. An X-ray beam of 0.65 mm height with an incidence angle of  $\theta = 5$  mrad illuminates the mirror surface over 130 mm, and has to be focused at a distance of  $q = 0.45$  m. A bending radius of  $R = 178.0$  m is expected at the centre of the mirror. Two picomotors (New Focus, model #8321, Santa Clara, CA 95051-0905, USA) have been used to drive the flexure bender. Test results show a photon flux gain of 500, thanks to the mirror focusing. The sensitivity in slope is  $0.1 \mu\text{rad}$ , and the r.m.s. residual slope error of the mirror is  $0.8 \mu\text{rad}$ .

This case has been studied both by the FEM and by using the bender driving equation (5) with the associated equations. The bending-loss factors from Table 1 are  $\delta = 0.24425$ ,  $\delta_x = 0.00165$ ; the two forces calculated by (10) and (11) are  $F_1 = 24.083$  N,  $F_2 = 35.171$  N. The mirror is moved down a distance of  $z_0 = 15.80 \mu\text{m}$  at the centre, and inclined by an angle of  $\theta_0 = 17.37 \mu\text{rad}$ . These two effects are not negligible, and should be corrected. The deformation of the bender and mirror from the FEM are plotted in Fig. 3. It shows that the rotating axes of the mirror bender assembly are located in the expected region. The flexural hinges are deformed with essentially angular motion. The maximum Von Mises stress in the assembly is 38.8 MPa, which is much smaller than the elastic limit of the material ( $\sigma_{0.2\%} = 790$  MPa). The maximum Von Mises stress in the mirror is 5.9 MPa, compared with the yield stress of the silicon crystal of about 40 MPa.

The residual slope errors,  $\Delta\text{slope}$ , and differential curvatures,  $\Delta z'/z'(0)$ , between the ideal ellipse (7) and the bender driving equation (5), and between the results of the FEM and (5) are plotted in Fig. 4. Excellent agreements have been observed between the results from the FEM and (5) in a range of 130 mm ( $|x| < 65$ ):  $\Delta\text{slope} \leq 0.05 \mu\text{rad}$  and  $\Delta z'/z'(0) \leq 0.5\%$ . The end effects (in the area of  $65 < |x| < 75$ ) are predicted by the FEM. The

Mirror: Si,  $t_{\text{mir}} = 10$  mm  
Flexure: steel,  $t_{\text{hinge}} = 0.14$  mm

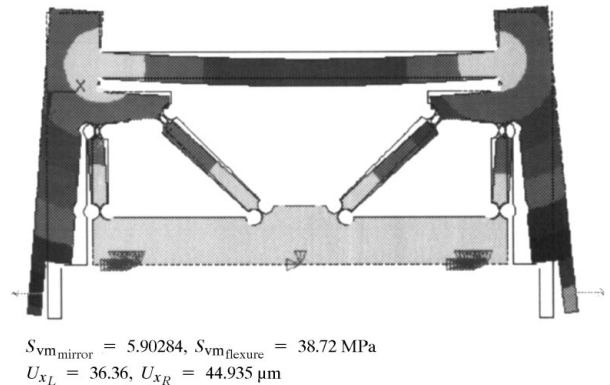


**Figure 3** Deformation of the bender and mirror by the FEM. Total forces applied by the two picomotors to the bender are  $F_1 = 24.083$  N,  $F_2 = 35.171$  N.

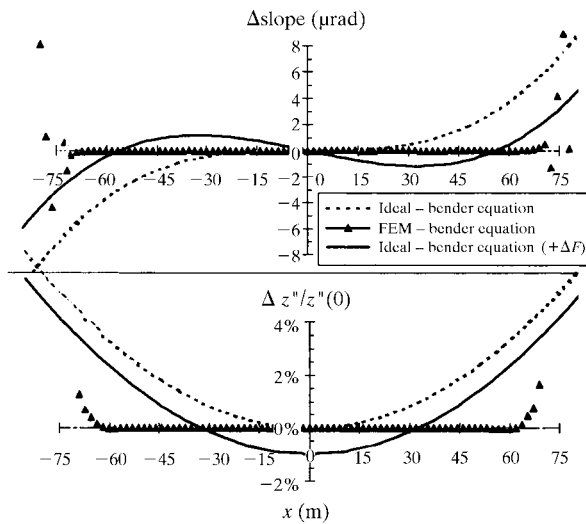


**Figure 4**

Residual slope error and differential curvature of a silicon mirror in an ellipse configuration:  $p = 40$  m,  $q = 0.45$  m,  $\theta = 5$  mrad. Additional force  $\Delta F_1 = \Delta F_2 = 0.238$  N.

residual slope errors and normalized differential curvatures between the bender equation and the ideal ellipse (Fig. 4) are clearly due to the quadratic term which is not generated by the flexure bender with the constant cross section of the mirror. The differences between the bender equation and the ideal ellipse in the range  $-65 < x < 65$  mm can be minimized by applying additional bending forces  $\Delta F_1 = \Delta F_2 = 0.238$  N:  $\Delta$ slope is reduced to 1.86  $\mu$ rad (r.m.s.  $\Delta$ slope to 0.76  $\mu$ rad) and  $\Delta z''/z''(0)$  to 3.0%. The minimized r.m.s. residual slope error is consistent with the test results (0.8  $\mu$ rad r.m.s.). These residual slope errors and differential curvature can theoretically be reduced to zero by using a variable cross section of the mirror.

The sensitivity of the slope to the displacement of the actuator was discussed in §2.4. Analysed results show that a displacement of 12 nm of the actuator generates a slope of 0.1  $\mu$ rad on the mirror. This agrees with the test results: 0.1  $\mu$ rad slope increment of the mirror while the two picomotors have an average step size of about 2 and 12 nm.

#### 4. Short-bending-radius applications

For the short-bending-radius applications, it is necessary to optimize the bending lever  $h$ , the mirror geometry (thickness  $t$  and width  $W$ ) and the material for the substrate. In general, the system should have (i) the neutral plane of the mirror placed on the rotating axes of the bender to minimize the bending-loss factors, (ii) a longer bending lever  $h$  for the bender, (iii) smaller thickness  $t$  and width  $W$  for the mirror, (iv) a lower Young's modulus  $E$  for the substrate.

The flexure bender was redesigned by integrating the above considerations. In particular, the bending lever  $h$  was increased from 92 to 200 mm, and the bender width  $W$  reduced from 50 to 30 mm. The expected minimum bending radius is  $R_0 = 46$  m for a

10 mm-thick and 30 mm-wide silicon mirror;  $R_0 = 30$  m for a silica mirror of the same dimensions. The bending lever  $h$  can be easily made longer to increase the bending capacity. The stiffness of the bending lever  $k_{\text{lever}}$  is adjustable to adapt different actuators by using, for instance, a spring between the picomotors and the bending levers.

#### 5. Conclusions

A flexure bender driven by two actuators has been studied by use of the FEM and the analytical formulation. The relationship between the mirror shape and the driving forces, the so-called bender driving equation, is established. For any requested mirror shape, the bender driving equation can be used to determine the values of the bending forces, to optimize the geometry and the material of the mirror, and to evaluate the residual slope error due to the bender. Parameter study and design optimization lead to the conclusion that the neutral plane of the mirror or multilayers had to be placed on the rotating axes of the flexure bender in order to reduce the bending capacity loss. Comparison of results for a prototype bender with a silicon mirror shows good agreement between FEM, the bender driving equation and the test results on an ESRF beamline. Analysis and test results confirm the microradian accuracy of the bent mirror

Many thanks go to P. Marion and Y. Dabin for stimulating suggestions and fruitful discussions during this study, and to A. Rommeveaux for the numerous LTP measurements.

#### References

- Freund, A. (1992). *Rev. Sci. Instrum.* **63**(1), 413–418.
- Henins, A. (1987). *Rev. Sci. Instrum.* **58**(7), 1173–1176.
- Hignette, O., Freund, A. & Chinchio, E. (1997). *Proc. SPIE*, **3152**, 188–189.
- Howells, M. R. (1995). *Opt. Eng.* **32**(8), 1981–1989.
- Howells, M. R. & Lunt, D. (1993). *Opt. Eng.* **34**(2), 410–417.
- Krisch, M. (1993). PhD thesis, ESRF, France.
- Müllender, S., Goulon, J., Loeffen, P. W., Marion, P., Filipponi, A. & Zhang, L. (1997). *J. Phys. IV*, **7**(C2), 317–318.
- Müllender, S., Marion, P., Zhang, L., Brookes, N. B. & Goulon, J. (1995). *Physica*, **B208/209**, 225–226.
- Padmore, H. A., Howells, M. R., Irick, S., Renner, T., Sandler, R. & Koo, Y. M. (1996). *Proc. SPIE*, **2856**, 145–157.
- Paros, L. M. & Weisbord, L. (1965). *Mach. Des.* **37**, 151–156.
- Signorato, R., Hignette, O. & Goulon, J. (1998). *J. Synchrotron Rad.* **5**, 797–800.
- Susini, J. (1992). *Proc. SPIE*, **1740**, 45–47.
- Susini, J., Labergerie, D. & Zhang, L. (1995). *Rev. Sci. Instrum.* **66**, 2229–2231.
- Ugural, A. C. & Fenster, S. K. (1995). *Advanced Strength and Applied Elasticity*. Englewood Cliffs: Prentice Hall.
- Young, W. C. (1989). *Roark's Formulas for Stress and Strain*, 6th ed. New York: McGraw-Hill.
- Zhang, L., Susini, J. & Labergerie, D. (1994). *J. Chin. Univ. Sci. Technol.* **25**, 219–224.
- Ziegler, E. (1995). *Opt. Eng.* **34**(2), 445–452.
- Ziegler, E., Hignette, O., Lingham, M. & Souvorov, A. (1996). *Proc. SPIE*, **2856**, 61–67.